Article

Determining the Self-Limiting Electrospray Deposition Compositional Limits for Mechanically Tunable Polymer Composites

Robert A. Green-Warren,[§] Luc Bontoux,[§] Noah M. McAllister, Dylan A. Kovacevich, Asaad Shaikh, Christianna Kuznetsova, Max Tenorio, Lin Lei, Assimina A. Pelegri, and Jonathan P. Singer*

Read Online

ACCESS | ⬚ Metrics & More | ⬚ Article Recommendations | ⬚ Supporting Information

ABSTRACT: Electrospray deposition (ESD) is a versatile micro-/nanocoating technology that utilizes the competition between the surface charge of a droplet and its surface tension to create monodisperse generations of micro-/nanodroplets. ESD can deposit uniform thin films by including dilute solutes in these droplets. One mode of ESD, self-limiting ESD (SLED), has been shown to exist when glassy polymers are sprayed in a volatile solvent below the polymer glass-transition temperature (T_g). This leads to charge accumulation on the coating surface that slows the growth of the film thickness. Since solutes can be easily blended in dilute ESD solutions, we investigate the SLED limits of self-limiting and non-self-limiting solute blends. As a motivating application, we focus on the mechanical properties of the films.

Specifically, we blend self-limiting polystyrene and SU-8 epoxy resin with different non-self-limiting mechanical modifiers, such as plasticizers and curing agents. To characterize the resulting morphologies and mechanical properties, we employ scanning electron microscopy and nanoindentation of the as-received porous and thermally smoothed films. The results illustrate the formation of composited polymers that exhibit self-limiting ability by SLED, depending on the interaction between the two components. Furthermore, mechanical properties could be effectively fine-tuned within these compositional ranges. This signifies that the 3D coating capabilities available through SLED can be enhanced by incorporating additional functionalities and properties beyond the base matrix.

KEYWORDS: *electrospray deposition, polymers, composites, nanoindentation, coatings*
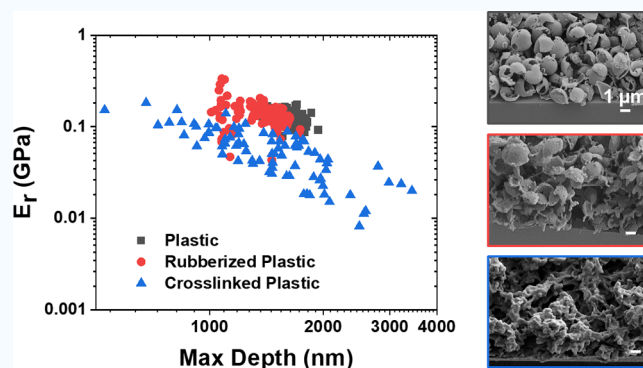
■ INTRODUCTION

The role of polymer thin films has been increasingly explored due to their application in modern engineering systems. Such applications include selective membranes for microfiltration systems, hydrophobic barriers for microelectronic devices, encapsulation of micro-/nanoscale biomedical devices, and separation membranes for energy storage systems. Many studies have considered nanoscale coatings produced conventionally by vapor deposition or electrodeposition. However, these methods require a fluid bath during the coating process or vacuum-based machinery and only work with a narrow selection of coating materials.[1,2] For more flexible brush-, dip-, and blade-coating approaches, poor coating process control leads to nonuniform coverage on both 2D and 3D targets due to capillary effects.[3−5]

Electrospray deposition (ESD) has been developed for micro-/nanoscale coatings in the past few decades[6−14] to reduce material waste and increase coating uniformity. ESD utilizes the competition between electrostatic force and surface tension of the solution to form a Taylor cone at the tip of a charged nozzle. Then, atomization of the solution produces microscale droplets when the voltage reaches a critical value. As the solvent evaporates during descension, the charged droplet reaches the Rayleigh limit and then transitions through Coulomb fission into nearly monodisperse child droplets. This transition is followed by repeated Coulomb fission events as the droplets approach the spraying target (shown in Figure 1a).[15] The diameter of a majority of the droplets produced in ESD from the Taylor cone jet has been correlated with the fluid properties and spray flow rate as[16]

$$d = \alpha \left(\frac{Q^3 \varepsilon_0 \rho}{\pi^4 \sigma \gamma} \right)^{1/6} + d_o \tag{1}$$
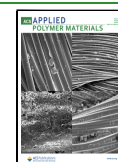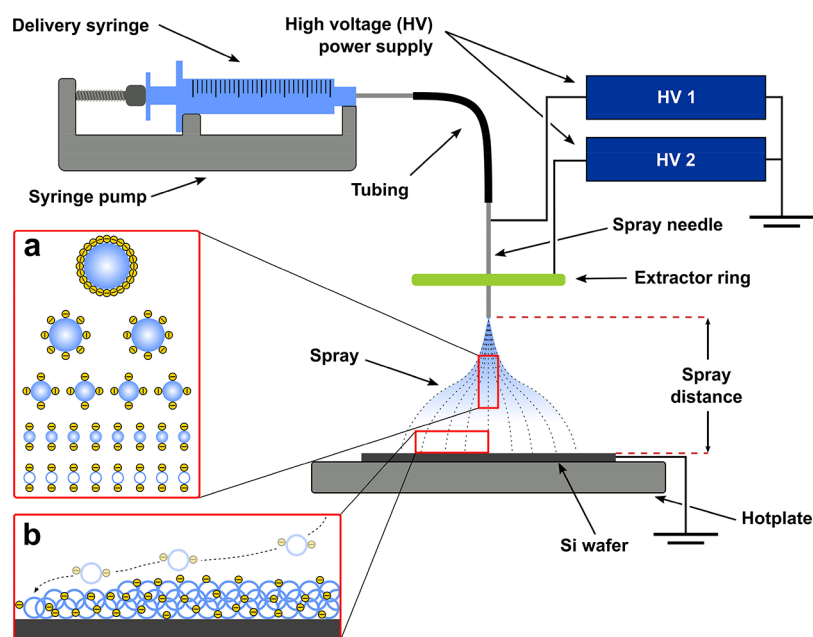
Figure 1. Schematic diagram of the ESD setup. (a) Coulombic fission process, where larger droplets are broken into monodisperse child droplets. (b) SLED process, where a buildup of surface charge redirects new droplets to uncoated areas of the target.

where α is a constant related to the fluid dielectric permittivity, ρ is the density, γ is the surface tension, σ is the electrical conductivity, Q is the flow rate, ε_0 is the permittivity of free space, and d_o is a small droplet diameter only significant at low flow rates.

Control of these parameters illustrates the advantages of this ESD over conventional coating techniques including the following: (1) the generation of monodisperse droplets resulting in a uniform deposition; (2) the final droplet size, which can be down to hundreds of nanometers, thereby highlighting ESD as an effective method for micro-/nanoscale coatings; (3) morphologies of thin films can be readily modified by adjusting the spray conditions, such as the flow rate; (4) the spray is efficiently delivered directly to the target without overcoat; and (5) the spray process can be accomplished in an ambient environment and at atmospheric pressure.[17]

An extension of ESD, coined self-limiting ESD (SLED), has been demonstrated by only spraying glassy insulating materials below their glass-transition temperature (T_g) and mixed with a volatile solvent onto a sufficiently conducting substrate.[18−24] A limited thickness that is proportional to the imposed electric-field strength[18] will be achieved as charges accumulate with increased spray time and spray is redirected to uncoated parts of the target (shown in Figure 1b). We have employed different polymers to investigate the mechanism of self-limiting through ESD. The results indicate that the critical thickness of SLED is determined by the total mass of sprayed polymer solids, the strength of the electric field, and the composition (e.g., dielectric strength, distance from T_g, and solvent affinity) of the spray solvent and polymer. Each of these parameters significantly impacts the thickness and morphology of thin films produced by SLED. For example, SLED coatings produced by in-air gelation of methylcellulose deliver nanowire SLED coatings as opposed to the rounded morphologies more frequently observed.[22] Notably, SLED allows for uniform coatings on complex 3D structures as a post-processing treatment,[18] including 3D-printed microlattices[19] and natural

structures.[22] However, the requirement for charge buildup does place limits on the composition of what can be employed in an SLED spray, which is the limitation we consider here.

Depositing blends through ESD is straightforward due to the ease of mixing dilute solutes. For example, the degree of crystallinity of the semiconducting polymer films prepared by ESD can be enhanced through modifying blending ratios.[25−27] In Hao et al.'s study, ESD was additionally employed to manufacture porous particles by blending drug and biodegradable polymers to precisely control the release rate of a drug.[8] More recently, Zhuang et al. investigated the use of ESD to produce a periosteum mimetic coating to enhance bone repair and reconstruction. In this study, poly(lactic-co-glycolic acid) and bone morphogenic protein-2, which mimics a peptide, are blended and deposited onto bone allografts.[28] Furthermore, Toth et al. took advantage of ESD's blending ability to create rapid, automated X-ray scattering evaluation of block copolymer compositional and experimental (e.g., temperature and film thickness) effects on the phase separation morphology.[29−31] Other than blending soluble polymers, solids have also been widely added to solutions for ESD. We have previously demonstrated that functional nanowires with tunable optical properties can be produced by spraying the composites of plasmonic nanoparticles and that they became better dispersed with the addition of a plasticizer.[22] While fabricating fuel-cell electrodes, the spray of blended catalyst particles and electrolytic solutions led to 3D nanostructures with large porosities and high surface areas, enhancing the device performance.[7,32,33] Most relevant for the current investigation, we employed polystyrene (PS) and styrenic block copolymers in a blended solution to change the surface properties of a 3D-printed hydrogel lattice.[19] The hydrogel coatings revealed that the non-self-limiting material blended with a self-limiting component maintains the ability to achieve uniform coatings on 3D complex structures. Additionally, swelling tests in this work demonstrated that the coating's mechanical properties, due to the plasticizing copolymer, were compliant enough to resist changes in the lattice size by up to

16%. This example illustrates that there exists a compositional limit of non-self-limiting and self-limiting blends to be still compatible with SLED and that there are functional benefits to exploring these blends.

Here, we investigate the SLED compositional limits of polymer blends through ESD. In this study, all samples were prepared by spraying composites with self-limiting and non-self-limiting components with various blending ratios. The immiscible blends include PS 35 kDa:Kraton D1102 (Kraton) and SU-8:soy oil. PS, a thermoplastic polymer with $T_g \approx 100$ °C, has been chosen as a model material with 2-butanone for obtaining SLED 3D coating in our previous work.[18] Kraton is a linear styrene−butadiene−styrene (SBS) triblock copolymer (BCP) with ~70 wt % butadiene ($T_g \approx -100$ °C) that is non-self-limiting and leads to the BCP being non-self-limiting, as we have previously shown.[19] Mechanically, Kraton can be used as a plasticizer for PS. SU-8 is an oligomeric epoxy resin that has a $T_g \approx 60$ °C. Oils are regularly used as resin plasticizers. Miscible composites include PS 850 Da:PS 35 kDa and SU-8:Versamid 125 (Versamid). PS 850 Da is chosen as a miscible plasticizer, having a T_g near room temperature.[34] Versamid is a reactive amide crosslinking agent that reacts with the epoxide groups in the SU-8 oligomer. Taken together from the standpoint of mechanical applications, we are examining the SLED behavior of two model plastics (PS and SU-8) with miscible (PS 35 kDa:PS 850 Da) and immiscible (PS 35 kDa:Kraton and SU-8:soy oil) plasticizers, along with a crosslinked plastic (SU-8:Versamid). The motivation for these selections is to mimic common coating formulation strategies for tuning mechanical properties. Transitions to self-limiting behavior were identified by evaluating changes in the central thickness after thermal smoothing of the film and visible appearance of the coatings. Porous and condensed samples prepared by SLED were examined by nanoindentation experiments to evaluate the mechanical properties of select composites.

■ EXPERIMENTAL SECTION

PS [molecular weight (MW) = 35 kDa and 850 Da, Sigma-Aldrich], Kraton D1102 (PolyOne GLS), SU-8 (EPON Resin SU-8), and soybean oil (Sigma-Aldrich) were used as received from the manufacturer. Versamid 125, a reactive polyamide resin, was used as a curing agent to make SU-8 composites. 2-Butanone (>99%, Sigma-Aldrich) was used as received as the carrier solvent for the spray solutions.

The schematic image of ESD is shown in Figure 1. The setup includes four main parts: (1) a syringe pump (KD Scientific), a stainless needle (Sai Infusion, 20 gauge, 1.5″), and (2) a steel extractor ring (inner diameter of 2 cm and an outer diameter of 4 cm) with (3) two negative high-voltage power supplies (Acopian) and (4) a 10 cm circular collection silicon wafer (University Wafer, boron-doped P-type 0−100 Ohm cm), placed in the center of the hotplate. The wafer was secured with an alligator clip attached to the ground wire during spray. Samples for nanoindentation tests were obtained by spraying 2.5 × 1 cm rectangular silicon chips.

In previous SLED studies, as well as a majority of other ESD works, positive polarity was employed. Negative-polarity sprays are occasionally used. For example, Tang et al. demonstrated the capability of negatively polarized electrospray particles to neutralize positively polarized electrosprayed particles and combine their payloads.[35] Here, negative polarity was chosen to confirm its ability SLED coatings and observe any resulting differences.

Silicon wafers and chips were cleaned and degreased by acetone and ethanol before spray. All of the precursor solutions for blend spray were made at 1 wt % and mixed in different ratios: 0:1, 1:5, 1:2,

1:1, 2:1, 5:1, and 1:0. Samples were sprayed for 60 min while setting the spray target distance to 4 cm, with a flow rate of 0.5 mL/h. The PS 35 kDa:PS 850 Da and PS 35 kDa:Kraton blends were sprayed at 35 °C to be more consistent with past results, and the SU-8:Versamid, SU-8:soy oil, and SU-8:PS 35 kDa blends were sprayed at room temperature (~20 °C) to avoid approaching the T_g of SU-8. The driving voltage in this work was set to approximately −5.4 kV. The stability of the Taylor cone was prioritized during spray: in sprays that were unstable at the nominal driving voltage (−5.4 kV), the driving voltage was set between −5.0 and −5.8 kV. The extractor ring was set ~1 cm above the needle tip, and the voltage was maintained between −2.7 and −3.3 kV. The Taylor-cone jet spray was utilized for all experiments in this study. The humidity was monitored and fell between 20 and 60% for each spray. To consistently measure sample thicknesses, samples were densified thermally above their flow points to remove any porosity present due to the particulate morphology. Densified PS and Kraton composite films were made by post-spray thermal treatment at 120 °C for ~10 s. To smooth SU-8:Versamid films for measuring thickness, samples were heated between 80 and 100 °C for ~10 s. The remainder of the crosslinking, as with the porous sample, was allowed to occur at room temperature. The experimental conditions for all samples can be found in Table S1.

A microscopic reflectometer (Filmetrics F40) and a motorized stage (Zaber E13F33E) were used to measure film thickness. To examine the self-limiting regime of samples, a linear mapping profile was collected using 200 points in a line, which covered the full range of the deposited film. The central 1 cm region of the profile was for calculating central thickness. The thickness of the chip samples for indentation tests was measured by mapping 100 points in a 10 × 10 square with 1 mm distance in the central 1 cm² of the film. For select samples, 45° cross-sectional imaging using Zeiss Sigma field-emission scanning electron microscopy (SEM) was employed to characterize the spray morphology. Samples were prepared by fracturing spray samples near the center of spray at room temperature with diamond scribe-prescribing. These samples were then mounted on 45° stubs.

The mechanical properties, including the reduced modulus E_r, work of deformation, and the ratio of elastic potential to total potential, of different polymer composites, was tested by using nanoindentation (Hysitron TI750 Ubi and NanoTest Vantage). The data obtained were analyzed using the native software packages included with the nanoindentation systems. This study utilized two nanoindenter tips: a Berkovich tip, defined as a three-sided self-similar pyramid with included angles of 65.3° from the vertical axis, and a cono-spherical tip with a radius of 10 μm for the Hysitron and Vantage, respectively. Indentations on the porous films were conducted on the Vantage with the cono-spherical tip to mitigate the effects of surface roughness and contact angle. The Hysitron was used to perform indents on the dense samples utilizing the Berkovich tip to minimize the indentation depth and to enable an earlier onset of plastic deformation.

To measure the mechanical properties via nanoindentation, load-controlled experiments were employed. In this regime, the nano-indenter goes into the material to a maximum specified load and the corresponding indentation depth is recorded. To avoid the artifacts associated with film−substrate interactions, single-indent depth-controlled experiments were initially performed to determine the maximum load at which ~10% of the film thickness was achieved during this indentation cycle. The load corresponding to this 10% depth was then prescribed as a maximum load during the actual experiment. A 5-2-5 load function with varying peak loads was used while keeping segment times constant. This load function represents a 5 s loading time, a 2 s hold time at the maximum load, and a 5 s unload time. For the unsmoothed samples, a 10 × 10 indentation grid with a constant 0.1 mN load was implemented for a total of 100 indents, each spaced 30 μm apart. However, for the smoothed samples, five 5 × 5 indentation grids, totaling 125 indents, were conducted at select locations on the film, with a grid spacing of 60 μm. Three of the five grids were completed with a constant load function, while the remaining two grids varied the load from 400 to 0 μN. This was done to ensure that the results were consistent across a
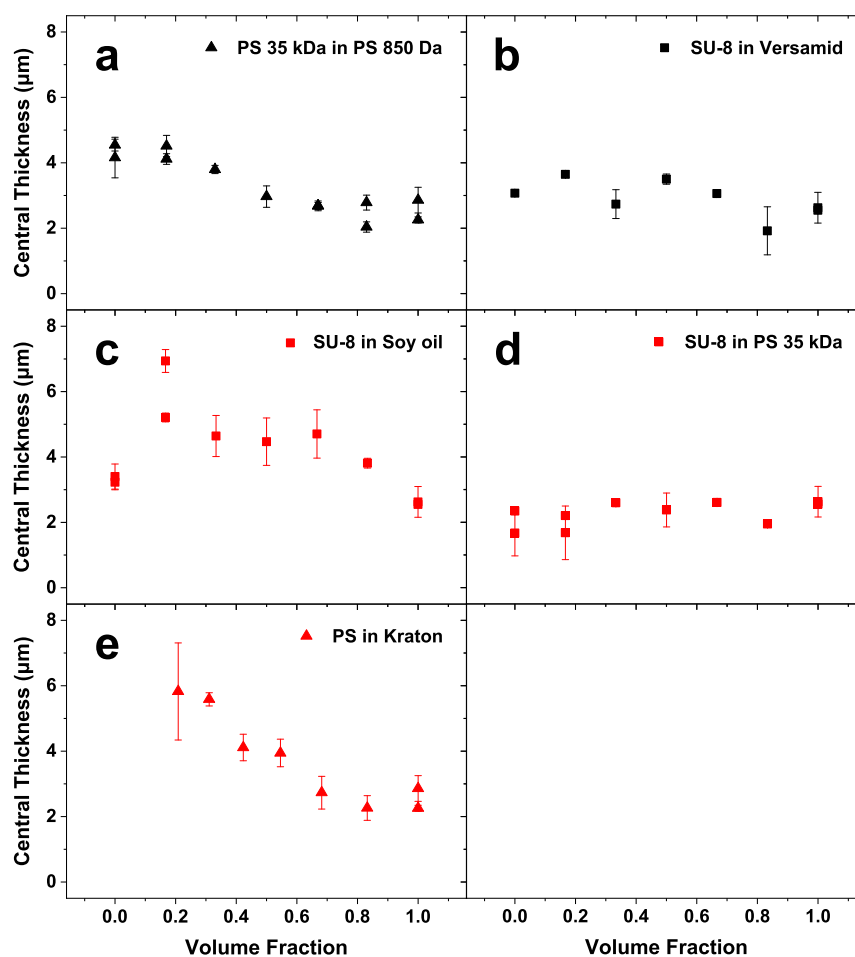
Figure 2. Measurements of film thickness after densification. (a,b) Miscible blends sprayed at different volume fractions: (a) PS 850 Da:PS 35 kDa and (b) SU-8:Versamid. (c−e) Immiscible blends sprayed at different volume fractions: (c) SU-8:soy oil, (d) SU-8:PS 35 kDa, and (e) PS 35 kDa:Kraton. In (e), the reported volume fraction considers the PS content in the Kraton SBS BCP. All blends were sprayed at 1 wt % solids at 0.5 mL/h for 60 min; (a,e) were sprayed at 35 °C and (b−d) were sprayed at room temperature (∼20 °C). Each data point represents the result of a single spray. The sixth panel is deliberately left blank.

range of depths. Three compositions, namely, pure PS 35 kDa, PS 35 kDa:Kraton (1:1), and SU-8:Versamid (2:1), were selected for nanoindentation testing. For each blend, both a porous and a densified sample were indented, leading to a total of six samples on which mechanical analysis was performed. Crosslinked samples were allowed to cure at room temperature for at least 24 h prior to measurement.

RESULTS

Our previous study demonstrated that 1 wt % diluted PS in 2-butanone sprayed at a flow rate of 0.5 mL/h and a substrate temperature of 35 °C at a distance of 4 cm was a condition, among others, that reliably displayed self-limiting results.[18] These spray conditions were used as the defaults to implement homogeneous and blended samples in this study; however, samples that contained SU-8 were sprayed at room temperature since SU-8's glass transition temperature is much lower than that of PS. The coating thickness of the blends was compared with the standard thickness-limited PS and SU-8 films in order to evaluate the self-limiting ability of the different blends. Figure 2 depicts the selected miscible and immiscible blends along with the central thickness of post-smoothed films plotted against the volume fraction of each substance. Photographs of pure material sprays and select transition-state samples can be found in Figure S1. Figure 2a,b shows two

miscible components deposited as blends. In Figure 2a, as the self-limiting PS 35 kDa was gradually added to non-self-limiting, charged melt PS 850 Da, the film thickness varies linearly from a pure PS 850 Da of 4.3 ± 0.3 μm to the SLED thickness of pure PS 35 kDa under these conditions (2.6 ± 0.4 μm), which should be noted to be statistically equivalent to the thickness obtained at positive polarity.[18] SU-8:Versamid composites in Figure 2b demonstrate a transition from a plateau near the electrowetted thickness (3.1 ± 0.1 μm) of pure Versamid to a pure SU-8 SLED thickness of 2.6 ± 0.3 μm.

For the spray of immiscible polymer blends in Figure 2c−e, the tendency of thickness variation becomes more complex than miscible blends. As Figure 2c illustrates, the thickness of pure sprayed soy oil transitions from electrowetting with a low thickness of 3.3 ± 0.3 μm to a rough charged melt regime (with a maximum average thickness at 0.167 volume fraction of 6.1 ± 0.3 μm) before reaching the self-limiting thickness of pure SU-8. In Figure 2d, the composites of PS 35 kDa and SU-8 maintain the ability to be self-limited irrespective of the variation in the volumetric ratio between the two materials due to each's self-limiting nature and the similarity of their self-limiting thicknesses. The only observable difference is a subtle minimum when the volume fraction of SU-8 was 80%. In
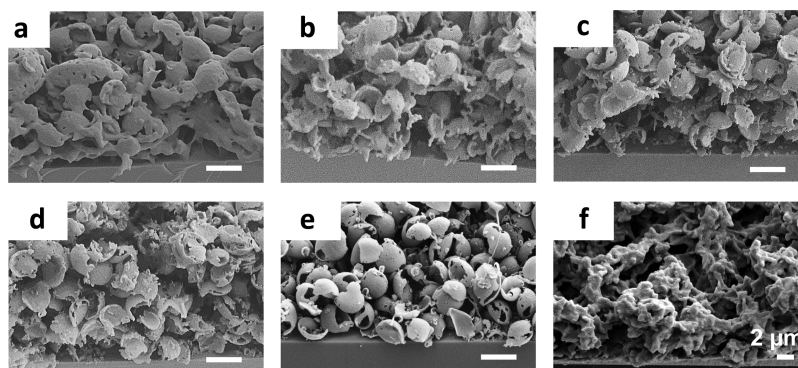
Figure 3. Cross-sectional SEM images of 1 wt % total solids of PS 35 kDa:Kraton and SU-8:Versamid of different ratios sprayed at 0.5 mL/h for 60 min at 35 °C. (a) 1:2 (PS 35 kDa:Kraton); (b) 1:1 (PS 35 kDa:Kraton); (c) 2:1 (PS 35 kDa:Kraton); (d) 5:1 (PS 35 kDa:Kraton); (e) 1:0 (PS 35 kDa:Kraton); and (f) 2:1 (SU-8:Versamid).

Figure 2e, the central thickness of Kraton is 5.8 ± 1.4 μm with large roughness typical of what we call a "charged melt" spray (Figure S1c). This regime is characterized by cellular electrostatic instabilities ("Taylor-Bènard cells"[18]) and has the smallest spot size of the insulating sprays measured here. With the addition of PS 35 kDa, the film thickness decreases in an apparent stepwise fashion again, showing either a plateau or minimum before reaching the SLED thickness of PS.

To demonstrate the change in microscale morphology, cross-sectional SEM was used. Figure 3a–f shows SEM images of 1 wt % PS 35 kDa with Kraton blend samples sprayed in different ratios. In Figure 3a, since the spray temperature is much higher than the T_g of the butadiene block of the BCP and there is only 36 wt % of the styrene fraction for sprayed droplets, the miscible blend forms a continuous porous film with only few hollow-shell structures on the surface. However, when the concentration of PS increased, the morphology of PS:Kraton composites varied from connected discs to more integrated spherical shells in Figure 3b–e. For the SU-8:Versamid blend, the crosslinking agent similarly plasticizes and fuses the deposited particles. The porous structure in Figure 3f indicates that the blend spray of SU-8:Versamid leads to a crosslinked porous network via ESD. Based on our observations, the fusing in the SU-8:Versamid films is a gradual process that continues after spray, with 1:1 ratios spraying as powder films before auto-leveling into optically dense films during the gradual crosslinking (Figure 4).
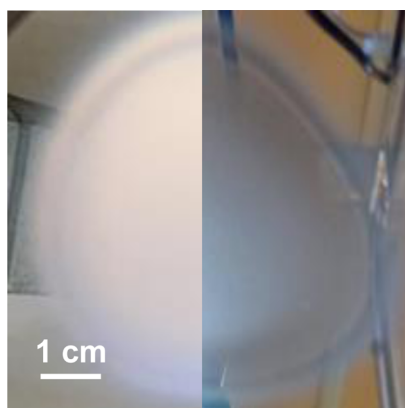

Figure 4. Photographs of an SU-8:Versamid 1:2 blend coating before (left) and after (right) 1 day of auto-leveling at room temperature as observed by a reduction in scattering.

Figure 5a–d shows the nanoindentation results of both porous and condensed sprayed thin films. Figure 5a shows that the reduced modulus, E_r, of porous films decreases as the indentation depth varies from 200 to 3750 nm. With the indent depth increasing, the reduced modulus of porous SU-8:Versamid changes from ~0.1 to ~0.01 GPa, and the value tends to be less than both the PS 35 kDa and PS 35 kDa:Kraton samples for comparable depth. At early indents, the smoothed SU-8:Versamid has a reduced modulus of 4.0 ± 1.3 GPa before reducing rapidly at higher loadings. Porous pure PS 35 kDa and PS 35 kDa:Kraton have similar moduli ~0.01 GPa, corresponding to each indentation depth. In Figure 5d, the smoothed pure PS 35 kDa thin film exhibited the highest reduced modulus of nearly 7.8 ± 0.4 GPa, which, while higher than may be expected for bulk PS, is similar to other confined PS films measured by indentation.[36] The smoothed PS 35 kDa:Kraton blend shows the lowest reduced modulus around 0.43 ± 0.05 GPa. Figure 5b,e shows the work done during nanoindentation tests. Figure 5b indicates that the SU-8:Versamid sample necessitates the most work to reach an indent depth of 1000 nm. Additionally, Figure 5b illustrates that the PS 35 kDa and PS 35 kDa:Kraton samples require a similar amount of work deformation for identical depths of indentation. Values of work on different samples seemed to increase linearly with indentation depth on a log–log scale. For condensed samples, the nanoindenter does the most work on the pure PS 35 kDa sample when compared to both SU-8:Versamid and PS 35 kDa:Kraton samples, as illustrated in Figure 5e.

■ DISCUSSION

While we have identified categories of ESD of glassy materials based on viscosity and charge dissipation, it is important to note that, for the most part, these classifications are continua. For example, in the case of the transition from electrowetting sprays to charged melt sprays, the balance of charge injection/dissipation and coating mobility determines whether it is more efficient to dissipate charge via electrostatic instability or wetting. This switch can even occur during the spray as the thickness of the coating makes it too difficult to dissipate charge through wetting. Such an example is PS 850 Da, which clearly displays both highly smooth and high-roughness regions at the edge and center of the spray, respectively (Figure S1f). However, the transition between self-limiting and a charged melt evinces that a powder becomes increasingly densified during the parameter change until it is better described as a
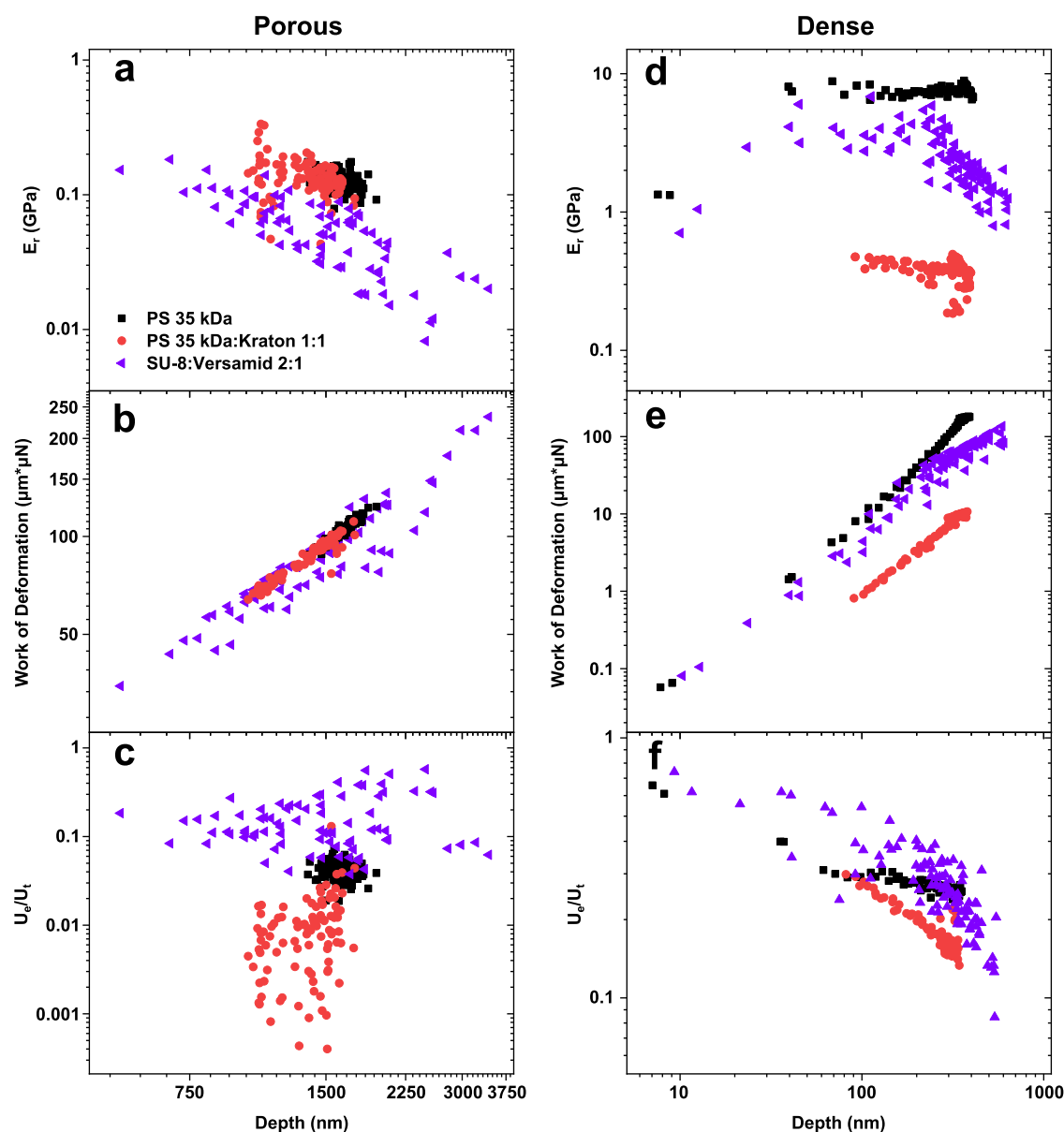
Figure 5. Nanoindentation results of porous (a−c) and condensed (d−f) blends created by ESD: (a,d) reduced modulus *vs* depth; (b,e) work of deformation *vs* depth; and (c,f) ratio of elastic potential to total potential *vs* depth.

viscous liquid. Optically, this can be observed as a reduction in scatter, as in SU-8:Versamid blends (Figures 4 and S1h). For miscible composites, adding a self-limiting component initiates this transformation gradually, with the visible transition to a powder coating appearing with less than 20 vol % self-limiting components added. This is similar to what was observed when increasing temperature in our previous work.[18] SEM results also confirm this transition through surface morphology changes to a fused shell assembly (Figure 3). The higher conductivity and solvent interaction of the polymer network with the polymer approaching its T_g allowed for enhanced charge dissipation. In other words, the mechanism of phenomenological changes in miscible blends spray is attributed to the added self-limiting components (PS 35 kDa, SU-8) increasing the T_g of blends. The pure self-limiting species also display different behaviors. The pure PS spray is more stable but thicker than the pure SU-8. Both of these effects are consistent with our past results with SU-8

possessing a higher dielectric constant but more facile solvent swelling and low glass transition due to the oligomeric nature of the substance.[20] It is interesting to note that the addition of either miscible or immiscible components does appear to stabilize the thickness of SU-8, which is suggestive that additives offset this sensitivity to solvent.

For immiscible blends, adding solid self-limiting components into liquid non-self-limiting materials displays more complex effects (Figure 2c,d). In the spray of SU-8:soy oil, the low-viscosity soybean oil goes from a near-electrowetting state to a thick-charged melt due to the addition of immobile glassy domains. After stabilizing at a charged melt thickness of ∼5 μm for a wide compositional range, the blend becomes more self-limiting and takes on a powdery appearance as the oil becomes dispersed in SU-8. In contrast, the composites of the two self-limiting components (Figure 2e) always lead to a self-limiting spray with a subtle local minimum in thickness observed when PS 35 kDa is first added to SU-8. We have previously observed

that, while SU-8 is sensitive to solvent, its higher dielectric strength leads to it being more self-limiting as a mask material.[20] Taken together with the fact that blending seems to stabilize SU-8 sprays to solvent effects, it follows that adding PS to SU-8 would improve the stability.

The BCP results echo many of these trends but in a stepwise fashion. The microphase separation that occurs within a BCP with strongly immiscible blocks results in thermodynamically determined ordered phases[37] and can be considered a confined version of the immiscible blend effects. In the pure Kraton case having high butadiene fraction ($T_g \approx -100$ °C), a thick charged melt was observed due to the viscous enhancement of the glassy PS inclusions, which at the starting fraction should be a combination of at the starting fraction micelles and partially formed cylinders. Adding PS to this mixture is expected to initially swell the PS domains, having little effect on the overall morphology.[38] Then, as the fractions approach one another, there is a step down in thickness that aligns with the nominal transition to lamellar morphology. Here, the low-T_g material and high-T_g are both continuous phases, leading to a self-limiting immobile state that is a relatively poor self-limiting material similar to pure SU-8. This can be seen in the morphology as a fused network of shells (Figure 3a). Increasing the amount of PS further results in a final step in thickness. The morphology most likely transitions to swollen BCP domains contained in a matrix of excess PS as the ability to expand the domains fails in favor of macrophase separation.[38] This breaks the continuity of the low-T_g phase, seen in the SEM as gradual definition being added to the shell network (Figure 3c−e) approaching the morphology of pure PS (Figure 3f). There may additionally be a small local minimum with the 5:1 PS 35 kDa:Kraton composition similar to the PS 35 kDa:SU-8 blends, but it is below the error threshold. However, this would likely correspond to a morphology of BCP micelles with a polybutadiene core in the PS matrix.

We evaluated the ability to tune mechanical properties of the composites by employing nanomechanical measurements. In the porous state, the reduced moduli of the PS and plasticized PS 35 kDa:Kraton composite are similar, while the SU-8-Versamid is lower and shows scatter associated with brittle failure. Once densified, the PS 35 kDa:Kraton becomes much less stiff relative to PS and the crosslinked epoxy also becomes less stiff, revealing the effects of the collapsed and fused porous structure caused by the compositing. While the plasticized composite is much softer than the PS, the porous form is more fused and collapsed, leading to a relatively higher apparent reduced modulus. All samples displayed power-law plastic energy deformation, as shown in Figure 5b,e.

Table 1 tabulates the power-law exponent equations fitted to the work of deformation plots for each material. Each of the

equation fits has R^2 values above, with pure PS achieving the best fit. The densification process increases the exponent, the degree of strain hardening, in each case by roughly a factor of 2. PS has the highest exponent due to its relative ability to resist indentation as a rigid, plastically deformable material, which is reduced by plasticization. In each sample, a dramatic increase in the stiffness can be seen after the sample has been densified. This is illustrated in Figure 5 when comparing plots b and e. The densified samples require nearly an order of magnitude more work to achieve indents of the same depth. This demonstrates the ability of the materials to dissipate energy in their porous state and store energy in their condensed state. The variation in the reduced modulus of the SU-8:Versamid 2:1 specimen points to apparent spatial variation in the stiffness across the surface of the sample, which is most likely due to the creation of brittle fractures in the crosslinked system. These cracks relieve stress and result in lower apparent reduced modulus but do not always occur, resulting in the scatter. This also limits the ability to prevent plastic deformation, leading to the lowest overall exponent.

Previously, the ratio of elastic indentation work to total indentation work has been employed to characterize the degree of energy dissipation of silicone rubber thin films.[39] Therefore, the lack of plasticity associated with the smoothed SU-8:Versamid is also illustrated in Figure 5c,f. The SU-8:Versamid 2:1 demonstrates the most elastic recovery of the three materials both before and after densifying. The high values of work of deformation for the SU-8:Versamid 2:1 can be explained by Figure 5c,f. The increased load needed to perform an indent causes the deformation work to be higher for an equally deep indent. This comparatively high load required for an indent of equal depth in SU-8:Versamid 2:1 is also reflected in its reduced modulus values.

■ CONCLUSIONS

We have established the capability to create self-limiting microcoatings through ESD of glassy polymers blended with nonglassy modifiers and the compositional limits of this blending to maintain the SLED effect. The results show that non-self-limiting modifiers of up to 40 vol % can be added without disrupting the self-limiting behavior. Furthermore, these modifiers can alter the mechanical properties. This presents the ability to tune the characteristic mechanical behavior (i.e., brittle, elastic, and plastic) and the observed contact response through the blending approach. By selecting composition, the mechanism of the mechanical response can be tuned, while the degree of densification, which can be controlled thermally through partial densification, can set the contact mechanics. Since these blends maintain the SLED effect, functional coating of 3D objects with selected mechanical properties can be manufactured for various applications. In the future, additional functional modifiers can be pursued, such as spatially selective crosslinking, tunable surface adhesion, as well as non-mechanical effects such as electrical or thermal conductivity, chemical activity, or optical modification.

■ ASSOCIATED CONTENT

Ⓢ Supporting Information

The Supporting Information is available free of charge at https://pubs.acs.org/doi/10.1021/acsapm.2c00106.

Table 1. Power Equations and R^2 Values for Each of the Materials in Both Porous and Densified States

	material	exponent	R^2
porous	PS 35 kDa	1.03	0.90
	PS 35 kDa:Kraton 1:1	0.96	0.93
	SU-8:Versamid 2:1	0.92	0.87
dense	PS 35 kDa	2.18	0.99
	PS 35 kDa:Kraton 1:1	1.96	0.96
	SU-8:Versamid 2:1	1.85	0.80

Experimental parameters and photographs of sprayed pure coatings and selected blends (PDF)

■ AUTHOR INFORMATION

Corresponding Author

Jonathan P. Singer − *Department of Mechanical and Aerospace Engineering, Rutgers University, Piscataway, New Jersey 08854, United States;* orcid.org/0000-0002-5934-8795; Email: Jonathan.singer@rutgers.edu

Authors

Robert A. Green-Warren − *Department of Mechanical and Aerospace Engineering, Rutgers University, Piscataway, New Jersey 08854, United States*

Luc Bontoux − *Department of Mechanical and Aerospace Engineering, Rutgers University, Piscataway, New Jersey 08854, United States*

Noah M. McAllister − *Department of Mechanical and Aerospace Engineering, Rutgers University, Piscataway, New Jersey 08854, United States*

Dylan A. Kovacevich − *Department of Mechanical and Aerospace Engineering, Rutgers University, Piscataway, New Jersey 08854, United States*

Asaad Shaikh − *Department of Mechanical and Aerospace Engineering, Rutgers University, Piscataway, New Jersey 08854, United States*

Christianna Kuznetsova − *Department of Mechanical and Aerospace Engineering, Rutgers University, Piscataway, New Jersey 08854, United States*

Max Tenorio − *Department of Mechanical and Aerospace Engineering, Rutgers University, Piscataway, New Jersey 08854, United States*

Lin Lei − *School of Materials Science and Engineering, Chongqing Jiaotong University, Chongqing 400074, China*

Assimina A. Pelegri − *Department of Mechanical and Aerospace Engineering, Rutgers University, Piscataway, New Jersey 08854, United States*

Complete contact information is available at:
https://pubs.acs.org/10.1021/acsapm.2c00106

Author Contributions

§R.A.G.-W. and L.B. contributed equally to this work. The manuscript was written through contributions of all authors. All authors have approved the final version of the manuscript.

Notes

The authors declare no competing financial interest.

■ REFERENCES

(1) Jung, Y. C.; Bhushan, B. Mechanically Durable Carbon Nanotube−Composite Hierarchical Structures with Superhydrophobicity, Self-Cleaning, and Low-Drag. *ACS Nano* **2009**, *3*, 4155−4163.

(2) Zhang, Y.; Zhang, L.; Zhou, C. Review of chemical vapor deposition of graphene and related applications. *Acc. Chem. Res.* **2013**, *46*, 2329−2339.

(3) Brinker, C. J.; Frye, G. C.; Hurd, A. J.; Ashley, C. S. Fundamentals of sol-gel dip coating. *Thin Solid Films* **1991**, *201*, 97−108.

(4) Nguyen, D. D.; Tai, N.-H.; Lee, S.-B.; Kuo, W.-S. Superhydrophobic and superoleophilic properties of graphene-based sponges fabricated using a facile dip coating method. *Energy Environ. Sci.* **2012**, *5*, 7908−7912.

(5) Pierre, A.; Sadeghi, M.; Payne, M. M.; Facchetti, A.; Anthony, J. E.; Arias, A. C. All-printed flexible organic transistors enabled by surface tension-guided blade coating. *Adv. Mater.* **2014**, *26*, 5722−5727.

(6) Morozov, V. N.; Morozova, T. Y. Electrospray deposition as a method to fabricate functionally active protein films. *Anal. Chem.* **1999**, *71*, 1415−1420.

(7) Martin, S.; Garcia-Ybarra, P. L.; Castillo, J. L. Electrospray deposition of catalyst layers with ultra-low Pt loadings for PEM fuel cells cathodes. *J. Power Sources* **2010**, *195*, 2443−2449.

(8) Hao, S.; Wang, Y.; Wang, B.; Deng, J.; Zhu, L.; Cao, Y. Formulation of porous poly(lactic-co-glycolic acid) microparticles by electrospray deposition method for controlled drug release. *Mater. Sci. Eng. C* **2014**, *39*, 113−119.

(9) Xie, J.; Tan, J. C.; Wang, C.-H. Biodegradable films developed by electrospray deposition for sustained drug delivery. *J. Pharm. Sci.* **2008**, *97*, 3109−3122.

(10) Hu, H.; Singer, J. P.; Osuji, C. O. Morphology development in thin films of a lamellar block copolymer deposited by electrospray. *Macromolecules* **2014**, *47*, 5703−5710.

(11) Hu, H.; Rangou, S.; Kim, M.; Gopalan, P.; Filiz, V.; Avgeropoulos, A.; Osuji, C. O. Continuous equilibrated growth of ordered block copolymer thin films by electrospray deposition. *ACS Nano* **2013**, *7*, 2960−2970.

(12) Kim, J.-W.; Yamagata, Y.; Kim, B. J.; Higuchi, T. Direct and dry micro-patterning of nano-particles by electrospray deposition through a micro-stencil mask. *J. Micromech. Microeng.* **2009**, *19*, 025021.

(13) Steipel, R. T.; Gallovic, M. D.; Batty, C. J.; Bachelder, E. M.; Ainslie, K. M. Electrospray for generation of drug delivery and vaccine particles applied in vitro and in vivo. *Mater. Sci. Eng. C* **2019**, *105*, 110070.

(14) Shlyapnikov, Y. M.; Shlyapnikova, E. A.; Morozov, V. N. Reversible and Irreversible Mechanical Damaging of Large Double-Stranded DNA upon Electrospraying. *Anal. Chem.* **2016**, *88*, 7295−7301.

(15) Jaworek, A.; Sobczyk, A. T. Electrospraying route to nanotechnology: an overview. *J. Electrost.* **2008**, *66*, 197−219.

(16) Gañán-Calvo, A. M.; Dávila, J.; Barrero, A. Current and droplet size in the electrospraying of liquids. Scaling laws. *J. Aerosol Sci.* **1997**, *28*, 249−275.

(17) Matsumoto, H.; Mizukoshi, T.; Nitta, K.; Minagawa, M.; Tanioka, A.; Yamagata, Y. Organic/inorganic hybrid nano-micro-structured coatings on insulated substrates by electrospray deposition. *J. Colloid Interface Sci.* **2005**, *286*, 414−416.

(18) Lei, L.; Kovacevich, D. A.; Nitzsche, M. P.; Ryu, J.; Al-Marzoki, K.; Rodriguez, G.; Klein, L. C.; Jitianu, A.; Singer, J. P. Obtaining Thickness-Limited Electrospray Deposition for 3D Coating. *ACS Appl. Mater. Interfaces* **2018**, *10*, 11175−11188.

(19) Kovacevich, D. A.; Lei, L.; Han, D.; Kuznetsova, C.; Kooi, S. E.; Lee, H.; Singer, J. P. Self-Limiting Electrospray Deposition for the Surface Modification of Additively Manufactured Parts. *ACS Appl. Mater. Interfaces* **2020**, *12*, 20901−20911.

(20) Lei, L.; Gamboa, A. R.; Kuznetsova, C.; Littlecreek, S.; Wang, J.; Zou, Q.; Zahn, J. D.; Singer, J. P. Self-limiting electrospray deposition on polymer templates. *Sci. Rep.* **2020**, *10*, 17290.

(21) Bodnár, E.; Rosell-Llompart, J. Growth dynamics of granular films produced by electrospray. *J. Colloid Interface Sci.* **2013**, *407*, 536−545.

(22) Lei, L.; Chen, S.; Nachtigal, C. J.; Moy, T. F.; Yong, X.; Singer, J. P. Homogeneous gelation leads to nanowire forests in the transition between electrospray and electrospinning. *Mater. Horiz.* **2020**, *7*, 2643−2650.

(23) Zhu, Y.; Chiarot, P. R. Surface charge accumulation and decay in electrospray printing. *J. Phys. D: Appl. Phys.* **2020**, *54*, 075301.

(24) Zhu, Y.; Chiarot, P. R. Structure of nanoparticle aggregate films built using pulsed-mode electrospray atomization. *J. Mater. Sci.* **2019**, *54*, 6122−6139.

(25) Nasir, M.; Matsumoto, H.; Minagawa, M.; Tanioka, A.; Danno, T.; Horibe, H. Preparation of PVDF/PMMA blend nanofibers by electrospray deposition: effects of blending ratio and humidity. *Polym. J.* **2009**, *41*, 402−406.

(26) Pitsalidis, C.; Pappa, A. M.; Hunter, S.; Laskarakis, A.; Kaimakamis, T.; Payne, M. M.; Anthony, J. E.; Anthopoulos, T. D.; Logothetidis, S. High mobility transistors based on electrospray-printed small-molecule/polymer semiconducting blends. *J. Mater. Chem. C* **2016**, *4*, 3499−3507.

(27) Liao, Y.; Fukuda, T.; Takagi, K.; Kamata, N.; Fukuda, F.; Furukawa, Y. High crystallinity parameter poly(3-hexylthiophene-2,5-diyl) thin film fabricated by the electrospray deposition method. *Thin Solid Films* **2014**, *554*, 132−136.

(28) Zhuang, Z.; John, J. V.; Liao, H.; Luo, J.; Rubery, P.; Mesfin, A.; Boda, S. K.; Xie, J.; Zhang, X. Periosteum Mimetic Coating on Structural Bone Allografts via Electrospray Deposition Enhances Repair and Reconstruction of Segmental Defects. *ACS Biomater. Sci. Eng.* **2020**, *6*, 6241−6252.

(29) Toth, K.; Osuji, C. O.; Yager, K. G.; Doerk, G. S. Electrospray deposition tool: Creating compositionally gradient libraries of nanomaterials. *Rev. Sci. Instrum.* **2020**, *91*, 013701.

(30) Toth, K.; Osuji, C. O.; Yager, K. G.; Doerk, G. S. High-throughput morphology mapping of self-assembling ternary polymer blends. *RSC Adv.* **2020**, *10*, 42529−42541.

(31) Toth, K.; Bae, S.; Osuji, C. O.; Yager, K. G.; Doerk, G. S. Film Thickness and Composition Effects in Symmetric Ternary Block Copolymer/Homopolymer Blend Films: Domain Spacing and Orientation. *Macromolecules* **2021**, *54*, 7970−7986.

(32) Varga, Á.; Brunelli, N. A.; Louie, M. W.; Giapis, K. P.; Haile, S. M. Composite nanostructured solid-acid fuel-cell electrodes via electrospray deposition. *J. Mater. Chem.* **2010**, *20*, 6309−6315.

(33) Chaparro, A.; Gallardo, B.; Folgado, M.; Martín, A.; Daza, L. PEMFC electrode preparation by electrospray: optimization of catalyst load and ionomer content. *Catal. Today* **2009**, *143*, 237−241.

(34) Claudy, P.; Létoffé, J. M.; Camberlain, Y.; Pascault, J. P. Glass transition of polystyrene versus molecular weight. *Polym. Bull.* **1983**, *9*, 208−215.

(35) Tang, J.; Liu, W.; Wang, H.; Gomez, A. High Performance Metal Oxide-Graphene Hybrid Nanomaterials Synthesized via Opposite-Polarity Electrosprays. *Adv. Mater.* **2016**, *28*, 10298−10303.

(36) Chung, P. C.; Glynos, E.; Green, P. F. The Elastic Mechanical Response of Supported Thin Polymer Films. *Langmuir* **2014**, *30*, 15200−15205.

(37) Bates, F. S.; Fredrickson, G. H. Block Copolymer Thermodynamics: Theory and Experiment. *Annu. Rev. Phys. Chem.* **1990**, *41*, 525−557.

(38) Jeong, U.; Ryu, D. Y.; Kho, D. H.; Lee, D. H.; Kim, J. K.; Russell, T. P. Phase Behavior of Mixtures of Block Copolymer and Homopolymers in Thin Films and Bulk. *Macromolecules* **2003**, *36*, 3626−3634.

(39) Han, C.-S. Indentation size effect in polymers. In *Advances in Materials Science Research*; Nova Science Publishers, Inc., 2011; Vol. 10, pp 393−413.

⬚ Recommended by ACS